Vestibular role of KCNQ4 and KCNQ5 K+ channels revealed by mouse models

Spitzmaul, G. and Tolosa, L. and Winkelman, B.H.J. and Heidenreich, M. and Frens, M.A. and Chabbert, C. and de Zeeuw, C.I. and Jentsch, T.J.

Journal of Biological Chemistry
2013 MAR 29 ; 288(13): 9334-9344
Doi: 10.1074/jbc.M112.433383

American Society for Biochemistry and Molecular Biology

THE JOURNAL OF BIOLOGICAL CHEMISTRY VOL. 288, NO. 13, pp. 9334–9344, March 29, 2013

Vestibular Role of KCNQ4 and KCNQ5 K^+ Channels Revealed by Mouse Models*[S]

Received for publication, November 2, 2012, and in revised form, February 1, 2013 Published, JBC Papers in Press, February 13, 2013, DOI 10.1074/jbc.M112.433383

Guillermo Spitzmaul[‡1], Leonardo Tolosa[§2], Beerend H. J. Winkelman[§2], Matthias Heidenreich[‡3], Maarten A. Frens[¶], Christian Chabbert[‖], Chris I. de Zeeuw[§¶4], and Thomas J. Jentsch[‡5]**

*From the [‡]Leibniz-Institut für Molekulare Pharmakologie (FMP) and Max-Delbrück-Centrum für Molekulare Medizin (MDC), 13125 Berlin, Germany, the [§]Netherlands Institute for Neuroscience, 1105 BA Amsterdam, The Netherlands, the [¶]Department of Neuroscience, Erasmus MC, 3000 CA Rotterdam, The Netherlands, [‖]INSERM U1051 Institut des Neurosciences de Montpellier, 30491 Montpellier cedex 5, France, and the **Cluster of Excellence NeuroCure, Charité-Universitätsmedizin, 10117 Berlin, Germany*

Background: KCNQ K^+ channels regulate neuronal excitability, and KCNQ4 mutations cause deafness.
Results: KCNQ4 and KCNQ5 expression in vestibular organ and the impact on vestibular function are investigated.
Conclusion: Both channels reside in postsynaptic calyx membranes of hair cells, and loss of KCNQ4 impairs vestibular function.
Significance: KCNQ4 may affect vestibular function because of a novel role in synaptic transmission.

The function of sensory hair cells of the cochlea and vestibular organs depends on an influx of K^+ through apical mechanosensitive ion channels and its subsequent removal over their basolateral membrane. The KCNQ4 (K_v7.4) K^+ channel, which is mutated in DFNA2 human hearing loss, is expressed in the basal membrane of cochlear outer hair cells where it may mediate K^+ efflux. Like the related K^+ channel KCNQ5 (K_v7.5), KCNQ4 is also found at calyx terminals ensheathing type I vestibular hair cells where it may be localized pre- or postsynaptically. Making use of *Kcnq4*$^{-/-}$ mice lacking KCNQ4, as well as *Kcnq4*$^{dn/dn}$ and *Kcnq5*$^{dn/dn}$ mice expressing dominant negative channel mutants, we now show unambiguously that in adult mice both channels reside in postsynaptic calyx-forming neurons, but cannot be detected in the innervated hair cells. Accordingly, whole cell currents of vestibular hair cells did not differ between genotypes. Neither *Kcnq4*$^{-/-}$, *Kcnq5*$^{dn/dn}$ nor *Kcnq4*$^{-/-}$/*Kcnq5*$^{dn/dn}$ double mutant mice displayed circling behavior found with severe vestibular impairment. However, a milder form of vestibular dysfunction was apparent from altered vestibulo-ocular reflexes in *Kcnq4*$^{-/-}$/*Kcnq5*$^{dn/dn}$ and *Kcnq4*$^{-/-}$ mice. The larger impact of KCNQ4 may result from its preferential expression in central zones of maculae and cristae, which are innervated by phasic neurons that are more sensitive than the tonic neurons present predominantly in the surrounding peripheral zones where KCNQ5 is found. The impact of postsynaptic KCNQ4 on vestibular function may be related to K^+ removal and modulation of synaptic transmission.

The vestibular organ senses gravitational forces and acceleration and provides essential sensory input for the control of body equilibrium, head orientation, and eye movements. Sensory hair cells (HCs)[6] in otholithic organs (utricle and sacculus) respond to gravitational forces and linear acceleration, whereas HCs in the cristae ampullares detect rotational acceleration. Both types of sensory end organ contain different classes of HCs named type I and type II. These classes are not only distinguished by their pattern of innervation, with calyx terminals ensheathing type I cells, but also by other characteristics like the expression of distinctive plasma membrane currents (1).

Vestibular sensory output depends not only on mechanosensitive ion channels located in the stereocilia of HCs, but also on ion channels present in both the basolateral membrane of HCs and in their cognate afferents. These channels may modulate receptor potentials, synaptic transmission, and neuronal excitability. At least two members of the KCNQ (K_v7) K^+ channel family (2, 3), KCNQ4 and KCNQ5, are found in the vestibular organ (4, 5). KCNQ4 is important for hearing (5, 6), is mutated in patients with dominant DFNA2 deafness (6), and modulates touch sensation (7). KCNQ4 displays a highly restricted expression pattern. In the cochlea, it is localized at the basal pole of outer hair cells (OHCs) that depolarize and eventually degenerate upon *Kcnq4* disruption (5). KCNQ4 is also found at basal poles of vestibular type I hair cells that are ensheathed by calyx synapses (5). However, its localization to pre- or postsynaptic membranes remains controversial (4, 8–12). Unlike cochlear OHCs, vestibular HCs do not degenerate in *Kcnq4*$^{-/-}$ mice (5),

* This work was supported by a grant from the Deutsche Forschungsgemeinschaft (Exc 257) and the Prix Louis-Jeantet de Médecine (to T. J. J.), by a stipend from the Alexander von Humboldt Foundation (to G. S.), by the Dutch Organization for Medical Sciences (ZonMw; to C. I. d. Z.), Life Sciences (ALW; to C. I. d. Z.), Senter (Neuro-Basic; to C. I. d. Z.), CEREBNET (to C. I. d. Z.), C7 programs of the European Community (to C. I. d. Z.), and ERC (European Research Council)-advanced grant (to C. I. d. Z.).
[S] This article contains supplemental Figs. S1–S3.
[1] Present address: Instituto de Investigaciones Bioquímicas de Bahía Blanca (INIBIBB) and Universidad Nacional del Sur (UNS), Bahía Blanca, Argentina.
[2] Both authors contributed equally to this work.
[3] Present address: Broad Institute, Massachusetts Institute of Technology, Cambridge, MA.
[4] To whom correspondence may be addressed concerning vestibulo-ocular assays: Dept. of Neuroscience, Erasmus MC, P.O. Box 2040, 3000 CA Rotterdam, The Netherlands. Tel.: 0031-10-7043-299; Fax: 0031-10-704-4734; E-mail: c.dezeeuw@erasmusmc.nl.
[5] To whom correspondence may be addressed: Leibniz-Institut für Molekulare Pharmakologie (FMP) and Max-Delbrück-Centrum für Molekulare Medizin (MDC), Robert-Rössle-Str. 10, 13125 Berlin, Germany. Tel.: 0049-30-9406-2961 or 2975; Fax: 0049-30-9406-2960; E-mail: jentsch@fmp-berlin.de.

[6] The abbreviations used are: HC, hair cell; dn, dominant negative; EPSP, excitatory postsynaptic potential; OHC, outer hair cell; VOR, vestibulo-ocular reflex.

but ~30% of patients with *KCNQ4* mutations display mild vestibular symptoms (13).

KCNQ5 is more broadly expressed than KCNQ4 (14, 15), yields similar currents, but lacks cochlear expression. In vestibular sensory epithelia (5) it partially overlaps with KCNQ4. Apart from the disappearance of an afterhyperpolarization current in hippocampal neurons (16), no phenotype has been described in *Kcnq5*$^{dn/dn}$ mice carrying a dominant negative mutation.

Using KCNQ mutant mouse models we now resolve the controversy surrounding the contribution of KCNQ4 and KCNQ5 to vestibular HC currents and determine their physiological relevance for the vestibular system. We found that neither channel is significantly expressed in adult vestibular HCs, but rather postsynaptically in calyx terminals where their expression partially overlaps. Accordingly, currents of vestibular HCs were unchanged upon gene disruption. Vestibulo-ocular reflexes were reduced both in *Kcnq4*$^{-/-}$ and *Kcnq4*$^{-/-}$/*Kcnq5*$^{dn/dn}$ double mutant mice, whereas only marginal effects were observed in *Kcnq5*$^{dn/dn}$ mice. The larger impact of *Kcnq4* disruption on vestibular function may be related to its preferential expression in the central zones of vestibular sensory epithelia.

EXPERIMENTAL PROCEDURES

Mouse Models and Genotyping—The generation of *Kcnq4*$^{-/-}$, *Kcnq4*$^{dn/dn}$, and *Kcnq5*$^{dn/dn}$ mice and their genotyping has been described previously (5, 16). KCNQ4 mouse models were initially kept in C3H/HeJ and *Kcnq5*$^{dn/dn}$ mice in C57BL/6 background. Double mutant mice were generated by crossing *Kcnq4*$^{-/-}$ and *Kcnq5*$^{dn/dn}$ mice. They were viable, fertile, and had no immediately apparent phenotype. They were kept and investigated in the mixed background. Subsequently, all mutant genotypes were obtained by breeding mice heterozygous for both genes. Mice of either sex were used for experiments.

Immunofluorescence and in Situ Hybridization—Mice (2–52 weeks old) were anesthetized and perfused with 4% paraformaldehyde in PBS. Inner ears were dissected from the temporal bones in PBS and processed for (i) whole mount, (ii) slice immunohistochemistry, or (iii) *in situ* hybridization. For (i) we carefully excised the utricle and semicircular canals, opened the membranous labyrinth, and removed the otoconial membrane from utricles. Tissues were postfixed in 4% paraformaldehyde, washed with PBS, and incubated in blocking solution (17) (3% normal goat serum, 2% BSA, and 0.5% Nonidet P-40 in PBS) overnight. Primary antibodies were incubated for 48 h in carrier solution (PBS containing 1.5% normal goat serum, 1% BSA, and 0.25% Nonidet P-40). Secondary antibodies diluted in carrier solution were incubated overnight. Tissues were mounted unflattened in Fluoromount-G (Southern Biotech). For (ii) and (iii), inner ears were postfixed and decalcified as described (18). Tissues were cut in 8–12-μm sections and kept at −20 °C (for ii) or −80 °C (for iii). For (ii), slices were blocked with BSA for 2 h and incubated with primary antibodies in carrier solution (12 h). Secondary antibodies were incubated for 2 h. For whole mount (i) and immunohistochemistry (ii) the following primary antibodies were used: rabbit anti-KCNQ4 (4), 1:150 for (i) and 1:200 for (ii); guinea pig anti-KCNQ4 (7), 1:100 for (i) and 1:200 for (ii); rabbit anti-KCNQ5 (16), 1:150 for (i); rabbit and guinea pig anti-KCNQ5-C1b (raised against residues 793–808), 1:100 for (i) and 1:200 for (ii); mouse anti-calretinin (Swant), 1:200 for (i) and 1:400 for (ii); mouse and rabbit anti-β-III-tubulin (Covance), 1:500 for (i) and (ii); and mouse anti-calbindin (Swant), 1:400 for (ii). Nuclei were stained with DAPI. Fluorescence-labeled secondary antibodies were obtained from Molecular Probes and used diluted 1:500 for (i) and 1:1000 for (ii). For *in situ* hybridization (iii), sense and antisense digoxigenin-UTP-labeled riboprobes (DIG RNA labeling Mix; Roche Applied Science) were generated with T7 or SP6 RNA polymerase (Roche Applied Science), respectively, from linearized mouse cDNA clones (bp 1114–1560 for *Kcnq4* and 1744–2352 for *Kcnq5*). *In situ* hybridization on inner ear cryosections was performed as described (19). Pictures were taken for (ii) by a confocal laser-scanning microscope (LSM510; Zeiss), analyzed off-line with ZEN 2009 light edition software (Zeiss), and assembled using Adobe Photoshop (Adobe Systems). Pictures for (iii) were taken with a Zeiss Axiophot or Zeiss Stemi-2000-c microscope.

Electrophysiology—Whole cell recordings were done on HCs from acutely dissected utricles that were perfused at 0.5 ml/min with oxygenated solution containing 137 mM NaCl, 5 mM KCl, 2 mM $CaCl_2$, 1 mM $MgCl_2$, 10 mM HEPES, 11 mM glucose, pH 7.4. The epithelium was cut transversally and anchored to the chamber floor with two pieces of glass, exposing the basolateral membrane of hair cells. Central and peripheral hair cells could not be easily distinguished in this semi-intact preparation. However, patches were mostly obtained in the central and adjacent areas of the exposed tissue which may span the whole striola and juxtastriola and a minor portion of extrastriola. Recordings were done with 3–4-megohm electrodes filled with 140 mM KCl, 5 mM NaCl, 10 mM HEPES, 10 mM glucose, 5 mM EGTA, 3 mM MgATP, 1 mM NaGTP, pH 7.3. Type I and type II HCs were characterized (20) by the presence or absence, respectively, of the $g_{K,L}$ conductance (1). Microscopic inspection further helped to identify HC classes.

Whole cell recordings were done using a Multiclamp 700B amplifier (Molecular Devices). After seal formation (>10 GΩ) onto the basolateral membrane of HCs and membrane disruption, we estimated membrane capacitance (C_m) and series resistance (R_s) from the decay of capacitive transients induced by a ±10-mV pulse from a holding potential of −80 mV. After cancellation of capacitive transients, R_s was compensated up to 85%. The resting potential was measured as the zero current voltage in the current clamp mode. Data analysis used pClamp 10 software (Molecular Devices) and Origin 7.5 (OriginLab). Data were sampled at 10 kHz and filtered at 2 kHz. The voltage clamp protocol started from a holding potential of −70 (for type II HCs) or −90 mV (for type I HCs), followed by a 50-ms pulse to −110 mV for type I HCs and −100 mV for type II HCs followed by test pulses of 200 ms between −110 and +40 mV for type I HC and −100 to +50 mV in type II HC in steps of 10 mV, and a constant step to −30 mV for tail currents. In statistical analysis, the number of cells is given by *n*, and number of animals by *N*.

Expression in Xenopus Oocytes and Two-electrode Voltage Clamping—*Xenopus* oocytes were obtained and injected as described (15). A final amount of 20 ng of cRNA/oocyte was injected for each condition. Oocytes were incubated 3–4 days at 17 °C and then examined by two-electrode voltage clamping using a Turbo Tec03 (NPI Electronics) amplifier and pClamp 8.0 software (Molecular Devices). The protocol consisted of 5-s steps from −110 to +50 mV in 10-mV increments from a holding potential of −80 mV.

Vestibulo-ocular Reflexes—The vestibulo-ocular reflex (VOR) was tested in four groups of adult mice including wild-type (WT, $n = 15$), *Kcnq4*$^{-/-}$ ($n = 13$), *Kcnq5*$^{dn/dn}$ ($n = 17$), and *Kcnq4*$^{-/-}$/*Kcnq5*$^{dn/dn}$ ($n = 13$). In each experimental group about half of the mice were male. Mice were prepared for chronic head-restrained experiments, as described (21). The experimental protocol was approved by the Animal Experimentation Committee (DEC) of the Royal Dutch Academy of Sciences (KNAW).

During the experiment the mouse was placed head-fixed in a holder tube on a vestibular motion platform (R2000 Rotopod; Parallel Robotic Systems Corporation). Left eye orientation was measured using video pupil tracking with a table fixed CCD camera (Pulnix TM-6710CL, 120 frames/s) and IR illumination (850-nm LED, 6.5-cm distance from the eye). Pilocarpine (2%) eye drops were applied before the experiment to limit pupil dilatation in darkness. Online image analysis was performed to extract the location of pupil edges and corneal light reflections using custom built software for Labview (National Instruments, Austin, TX). Angular eye velocity was computed offline using custom software written for Matlab (The Mathworks Inc., Natick, MA) using the algorithm outlined elsewhere (22, 23). Saccadic eye movements and nystagmus fast phases were removed using a 50°/s velocity threshold and 200-ms margins at each threshold crossing. Each mouse was accustomed to the setup and experimental paradigm in a period of up to 3 training days before the experimental data were collected.

The horizontal VOR was characterized in darkness and in the light using sinusoidal rotation about the yaw axis, using frequencies ranging between 1/16 and 4 Hz, presented in a sequence of increasing order. Peak velocity was held constant at 25°/s. The number of cycles ranged between 5 (at 1/16 Hz) and 60 at 4 Hz. Eye velocity amplitude and phase shift relative to head movement were calculated using multiple linear regression of eye velocity to in-phase and quadrature components of the stimulus velocity. Gain of the eye movement response was defined as the ratio between the eye velocity amplitude and the stimulus velocity amplitude. Phase shift is expressed in degrees; positive phase shifts indicate phase lead. *Error bars* represent the S.E. Circular statistics were used to compare phase values. Transfer function profiles were statistically compared using MANOVA for repeated measures (SPSS Statistics 17.0.).

RESULTS

Differential Distribution of KCNQ4 and KCNQ5 in Vestibular End Organs—Previous studies examining the distribution of KCNQ4 and KCNQ5 in vestibular end organs were performed only with WT animals (4, 8, 11). We now used three genetic mouse models to control immunohistochemical labeling and to explore potential cross-talk between the expression of both proteins. *Kcnq4*$^{-/-}$ mice lack the KCNQ4 protein, whereas *Kcnq4*$^{dn/dn}$ mice express a dominant negative KCNQ4 variant carrying a point mutation (G286S) in the pore-forming P-loop (5). It corresponds to a mutation of a DFNA2 patient with dominantly inherited hearing loss (6). *Kcnq5*$^{dn/dn}$ mice carry an equivalent mutation (G278S) in KCNQ5 (16). KCNQ5(G278S) does not yield currents. It exerts strong dominant negative effects on co-expressed KCNQ3 and KCNQ5 WT subunits with which it can form heterotetramers (6, 15, 16).

Labeling vestibular end organs with our antibodies revealed a differential distribution of KCNQ4 and KCNQ5 in both the otholithic organs (Fig. 1) and cristae (supplemental Fig. S1). As displayed for utricles in Fig. 1*A*, KCNQ4 was most highly expressed in the central striolar and the adjacent juxtastriolar regions. It extended at weaker expression levels to the adjacent extrastriola (Fig. 1, *A* and *J*). By contrast, KCNQ5 was found mainly in the extrastriola and extended at lower expression levels into the juxtastriola (Fig. 1, *B* and *K*). As described previously (4, 5), both KCNQ4 and KCNQ5 were found in calyx-like structures that ensheathe type I vestibular hair cells (Fig. 1, *J* and *K*). Calyces were co-labeled for KCNQ4 and KCNQ5 in the juxtastriolar and extrastriolar regions (Fig. 1*L*). Likewise, KCNQ4 was found in central, intermediate, and peripheral zones of the cristae ampullares, whereas KCNQ5 was expressed in intermediate and peripheral zones but was almost undetectable in central zones (supplemental Fig. S1, *A–C, J–L*).

Importantly, labeling for KCNQ4 was abolished in tissue from *Kcnq4*$^{-/-}$ mice (Fig. 1*D* and supplemental Fig. S1*D*), validating the specificity of our staining. Surprisingly, labeling for KCNQ5 was virtually abolished in utricles from *Kcnq5*$^{dn/dn}$ mice that express a full-length KCNQ5 protein carrying a single point mutation (Fig. 1*H*). A similar pattern was observed in cristae ampullares (supplemental Fig. S1, *H* and *N*). Besides validating our KCNQ5 antibody staining, this finding suggested that the mutant protein was unstable or incorrectly targeted.

The partially overlapping expression patterns of KCNQ4 and KCNQ5 (Fig. 1, *C* and *L*, and supplemental Fig. S1, *C* and *L*) suggested that they may form heteromeric channels *in vivo*, as has been reported for co-transfected Chinese hamster ovary cells (24). Using dominant negative mutants, including the one expressed in *Kcnq5*$^{dn/dn}$ mice, we confirmed these findings in the *Xenopus* oocyte system that allows a more quantitative control of co-expression levels (supplemental Fig. S2, *A* and *B*). Importantly, KCNQ4/5 heterotetramers did not yield higher currents than the respective homotetramers, contrasting with findings for KCNQ3-KCNQ5 (15, 16) and KCNQ2-KCNQ3 channels (25, 26). Hence, the disruption of *Kcnq4* should not decrease K^+ currents more than expected from a loss of KCNQ4 currents alone. On the other hand, instead of a compensatory up-regulation, we observed a mild, but consistent decrease of KCNQ5 labeling in *Kcnq4*$^{-/-}$ vestibular organs (Fig. 1*E*). This finding hints at a role of KCNQ4-KCNQ5 complexes in trafficking, anchoring, or stabilizing KCNQ5 at its target membrane. The loss of KCNQ5 current in *Kcnq4*$^{-/-}$ mice, however, is expected to be mild. This contrasts with the strong dominant negative effect of the KCNQ5^{dn} mutant which will suppress currents from all KCNQ4 subunits present in

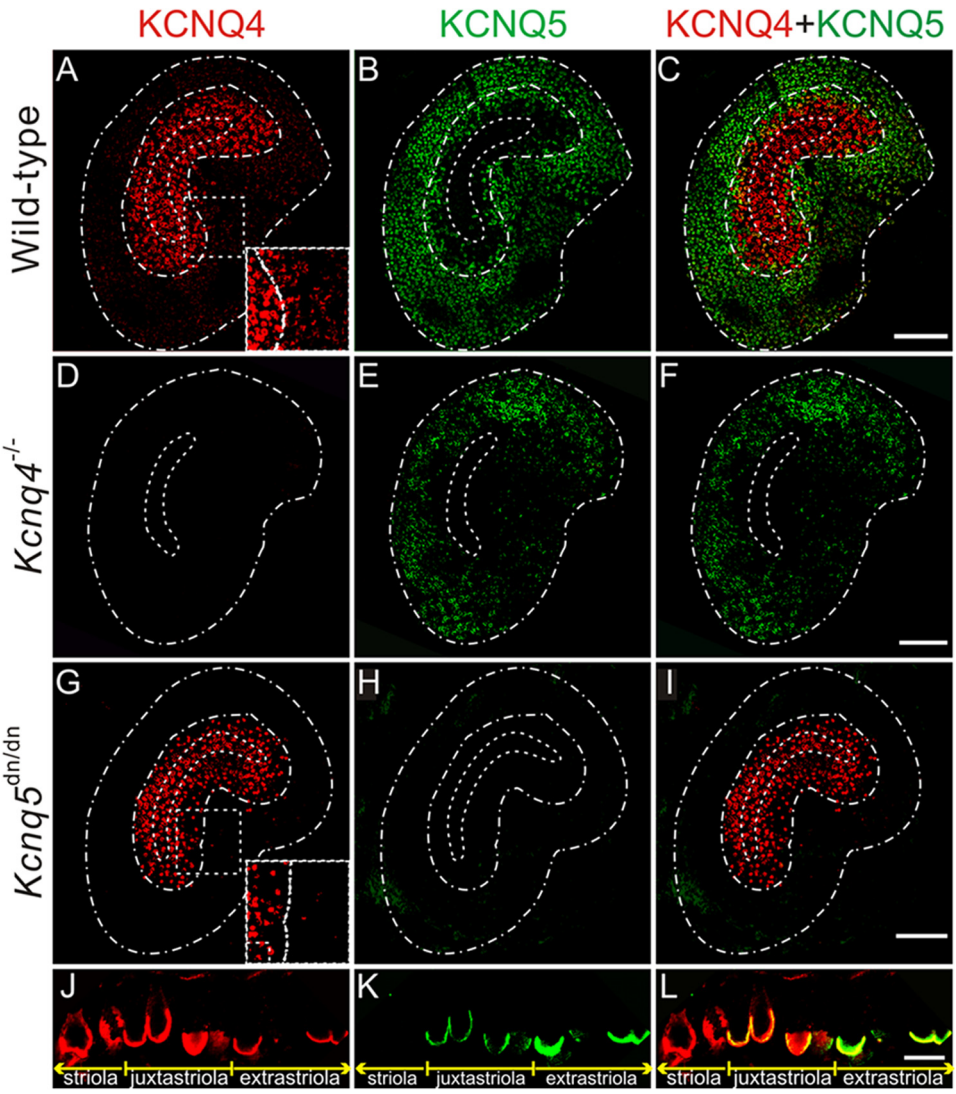

FIGURE 1. **Distribution of KCNQ4 and KCNQ5 in the mouse vestibular organ.** *A–I*, whole mount preparations of utricles from WT (*A–C*), *Kcnq4*$^{-/-}$ (*D–F*), and *Kcnq5*$^{dn/dn}$ (*G–I*) mice stained with antibodies against KCNQ4 (*left panel*) and KCNQ5 (*middle panel*). The merged signal is shown on the *right panel* (KCNQ4, *red*; KCNQ5, *green*). *Scale bars*, 100 μm. *Dashed white lines* in *A–I* indicate the approximate borders of the utricles (*outer line*), striola (*inner line*), and juxtastriola (*middle line*), except for *D–F* where the juxtastriola is not indicated due to the lack of KCNQ4 signal. The borders of the striola were taken from calretinin co-staining (data not shown). *Insets* in *A* and *G* show the area indicated by a *dashed line* at higher magnification and increased brightness to demonstrate that extrastriolar labeling for KCNQ4 is reduced in *Kcnq5*$^{dn/dn}$ mice. *J–L*, cross-section of a WT utricle labeled for KCNQ4 (*J*), KCNQ5 (*K*), and for both (merged) (*L*). The extension of the striola, juxtastriola, and extrastriola is indicated below. KCNQ4 and KCNQ5 expression overlaps in calyx terminals of the juxta- and extrastriola. Striolar calyces express only KCNQ4, which only in this region extends (at lower levels) further toward the apical opening of the calyx. *Scale bar*, 10 μm.

KCNQ4/5 heteromers. Of note, no dominant negative effect is expected in striolae (or central zones of cristae) as they lack appreciable KCNQ5 expression (Fig. 1, *B*, *E*, and *K*, and supplemental Fig. S1, *B* and *K*) (11). Hence, the output from the striola, which harbors the more sensitive, phasic HC-neurite complexes (27), will not be affected in *Kcnq5*$^{dn/dn}$ mice.

Neither KCNQ4 nor KCNQ5 Mediates Significant K^+ Currents in Adult Vestibular Hair Cells—The presence of KCNQ K^+ currents in vestibular type I and/or type II HCs was previously proposed based on their pharmacological and electrophysiological properties (5, 9, 28). To unambiguously determine the contributions of KCNQ4 and KCNQ5 to vestibular hair cell currents, we recorded whole cell currents from utricular hair cells from WT, *Kcnq4*$^{-/-}$, *Kcnq5*$^{dn/dn}$, and *Kcnq4*$^{-/-}$/*Kcnq5*$^{dn/dn}$ double mutant mice using the patch clamp technique. Because it was difficult to distinguish type I from type II HCs only by morphology, we used an established voltage protocol (20) to identify type I HCs by their characteristic $g_{K,L}$ K^+ current (29–31). This current had been hypothesized previously to be carried by KCNQ4 (4, 9). Contradicting this hypothesis, utricular type I HCs from 4–42-week-old mice of all genotypes under investigation (WT, *Kcnq4*$^{-/-}$, *Kcnq5*$^{dn/dn}$, and *Kcnq4*$^{-/-}$/*Kcnq5*$^{dn/dn}$) expressed large $g_{K,L}$ currents (Fig. 2, *A* and *B*, *left panels*). These currents were activated by depolarization, but were already partially active at the holding potential of −80 mV as shown by current deactivation upon an initial voltage step to −110 mV (Fig. 2*A*). There was no significant difference in those currents between the genotypes (Fig. 2*B*), and we observed no differences in resting potentials (WT: −76 ± 3 mV, S.E. $n = 7$; *Kcnq4*$^{-/-}$: −78 ± 3, $n = 5$; *Kcnq5*$^{dn/dn}$: −81 ± 3, $n = 4$; *Kcnq4*$^{-/-}$/*Kcnq5*$^{dn/dn}$: −80 ± 2, $n = 4$). Although KCNQ4 and KCNQ5 are mainly, if not exclusively,

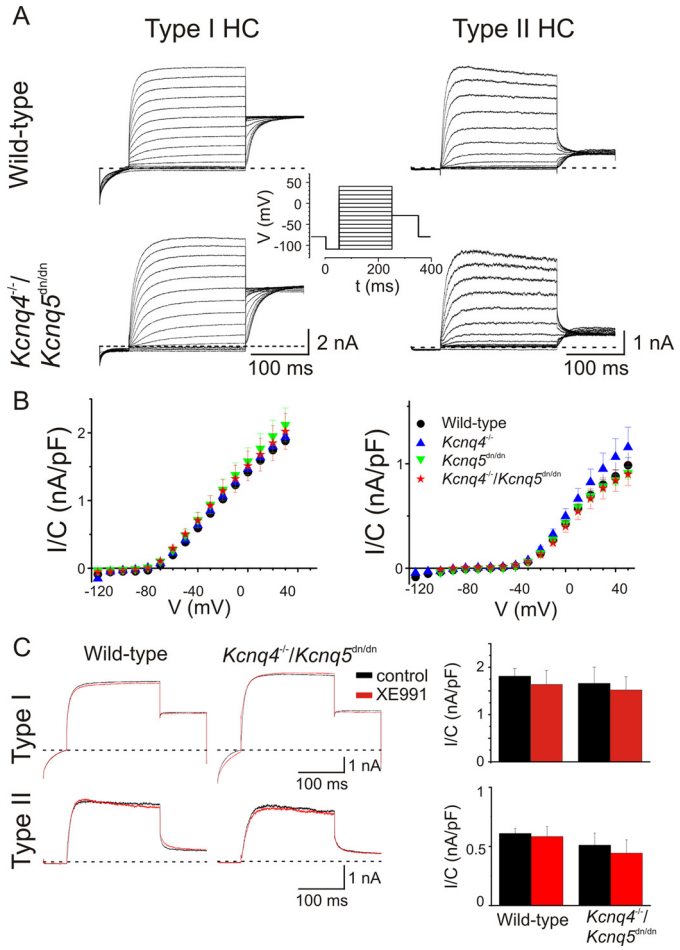

FIGURE 2. **Potassium currents from vestibular hair cell obtained from 4–42-week-old mice are not affected in mouse models for KCNQ4 and KCNQ5 channels.** *A*, potassium currents from type I (*left*) and type II HCs (*right*) obtained from semi-intact preparations of mouse utricle from wild-type and double-mutant mice *Kcnq4*$^{-/-}$/*Kcnq5*$^{dn/dn}$. *Insets* show voltage protocol used to obtain currents in type I and type II HCs, respectively. Cells were clamped before the voltage step to a −110 mV (type I HC) or −100 mV (type II HC) for 50 ms and after it to −30 mV. *B*, current-voltage relationship of potassium currents from type I (*left*) and type II (*right*) HCs for wild-type (*black dots*), *Kcnq4*$^{-/-}$ (*blue triangle*), *Kcnq5*$^{dn/dn}$ (*green triangle*), *Kcnq4*$^{-/-}$/*Kcnq5*$^{dn/dn}$ (*red star*) mice. Currents were normalized to cell capacitance. Number of measured cells from WT, *Kcnq4*$^{-/-}$, *Kcnq5*$^{dn/dn}$, and *Kcnq4*$^{-/-}$/*Kcnq5*$^{dn/dn}$ mice were 7, 5, 4, and 4 for type I HCs, and 26, 13, 4, and 5 for type II HCs, respectively. *C*, utricular type I (*upper panels*) and type II (*lower panels*) HC currents in the absence (*black traces*) and presence (*red traces*) of 10 μM XE991 perfused for 5 min after control trace. Currents were activated at +20 mV and obtained from wild-type (*left panel*) and *Kcnq4*$^{-/-}$/*Kcnq5*$^{dn/dn}$ (*middle panel*) mice. *Right diagrams*, averaged currents (at + 20 mV, and normalized to capacitance) for both genotypes. Numbers of animals were: type I HCs: n = 5 and 4 for wild-type and *Kcnq4*$^{-/-}$/*Kcnq5*$^{dn/dn}$ mice, respectively; and type II HCs: n = 6 for either wild-type or *Kcnq4*$^{-/-}$/*Kcnq5*$^{dn/dn}$ mice.

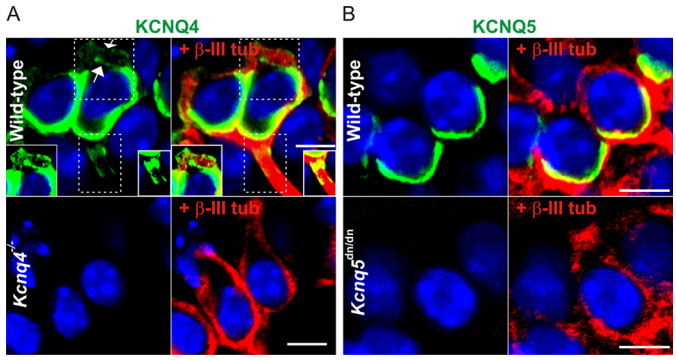

FIGURE 3. **Expression of KCNQ4 and KCNQ5 in type I hair cell calyces.** *A*, immunohistochemistry of striolar type I HC for KCNQ4 (*green*), counterstained for the nuclear marker DAPI (*blue*), and in *right panels* for β-III-tubulin (*red*), a cytosolic marker for calyces. *Top*, results from wild-type mice; *bottom panels*, from *Kcnq4*$^{-/-}$ mice. Note that weak KCNQ4 staining extends beyond the basal pole of the HC toward the neck of the calyx, where inner and outer membranes are labeled (*arrows*), and to the neurite. This is better visible in *insets* which show the areas enclosed by *dotted lines* with increased brightness. *Kcnq4*$^{-/-}$ sections are not labeled by the KCNQ4 antibody, demonstrating the specificity of staining. *B*, similar labeling for KCNQ5 of extrastriolar HCs. Note that KCNQ5 immunoreactivity does not extend beyond the basal part of the calyx and that labeling is abolished in *Kcnq5*$^{dn/dn}$ section. *Scale bars*, 5 μm.

expressed at calyx terminals of type I cells (4, 5), we also investigated type II cells in the same age range. They displayed the typical G_{DRII} current (1) and had a less negative resting voltage (−58 ± 3 mV, n = 26). As expected, we detected significant differences between genotypes neither in type II HC currents, nor in resting potentials (*Kcnq4*$^{-/-}$: −59 ± 2 mV, n = 13; *Kcnq5*$^{dn/dn}$: −57 ± 7 mV, n = 4; *Kcnq4*$^{-/-}$/*Kcnq5*$^{dn/dn}$: −59 ± 3 mV, n = 5). The half-maximal voltages of current activation ($V_{1/2}$) as determined from tail currents did not differ between the genotypes (supplemental Fig. S3, *A–C*). Moreover, 10 μM XE991, a potent blocker of KCNQ2, -3, -4, and -5 currents (15, 26, 32), failed to block K^+ currents of utricular type I or type II HCs from WT or *Kcnq4*$^{-/-}$/*Kcnq5*$^{dn/dn}$ mice (Fig. 2*C*). Hence, neither KCNQ4 nor KCNQ5 mediates significant currents in vestibular hair cells of mice older than 3 weeks.

KCNQ4 and KCNQ5 Are Not Expressed in Adult Vestibular Hair Cells, but in Afferent Neurons—The lack of KCNQ-mediated currents in >3-week-old type I HCs suggested that KCNQ4 and -5 are not expressed in those sensory cells, but rather reside in postsynaptic calyx membranes that ensheathe type I HCs. Confocal light microscopy cannot resolve the postsynaptic inner calyx membrane from the closely apposed basal, presynaptic HC membrane. A postsynaptic localization of KCNQ4, however, is strongly suggested by the extension of weaker KCNQ4 immunoreactivity along the outer calyx membrane into neurites (4, 11), a finding we now confirmed by *Kcnq4*$^{-/-}$-controlled immunostaining of striolar calyces (Fig. 3*A*). By contrast, KCNQ5 labeling (controlled by *Kcnq5*$^{dn/dn}$ HCs) was detected neither in outer calyceal membranes, nor in neurites (Fig. 3*B*). We correlated these findings with immunodetection of either channel protein in neuronal cell bodies of the vestibular ganglion (Fig. 4). Whereas somata of a neuronal subpopulation showed plasma membrane and intracellular labeling for KCNQ4 (Fig. 4*A*), KCNQ5 was not, or only barely, detectable (Fig. 4*D*). Hence, KCNQ5 may be more stringently targeted to the inner calyx membrane than KCNQ4. In *Kcnq5*$^{dn/dn}$ mice, however, KCNQ5 was detected in a punctate pattern in neuronal cell bodies (Fig. 4*F*), while disappearing from vestibular end organs (Fig. 1*H* and supplemental Fig. S1, *H* and *N*). Such a trafficking defect might also be expected for KCNQ4-KCNQ5 heteromers containing KCNQ5(G78S) subunits. Indeed, juxtastriolar and extrastriolar KCNQ4 labeling was mildly reduced in maculae and cristae of *Kcnq5*$^{dn/dn}$ mice (Fig. 1, *A* and *G*, and supplementary Fig. S1*M*). This reduction was more evident in the extrastriola where the KCNQ5/KCNQ4 ratio is larger (*insets* in Fig. 1, *A* and *G*).

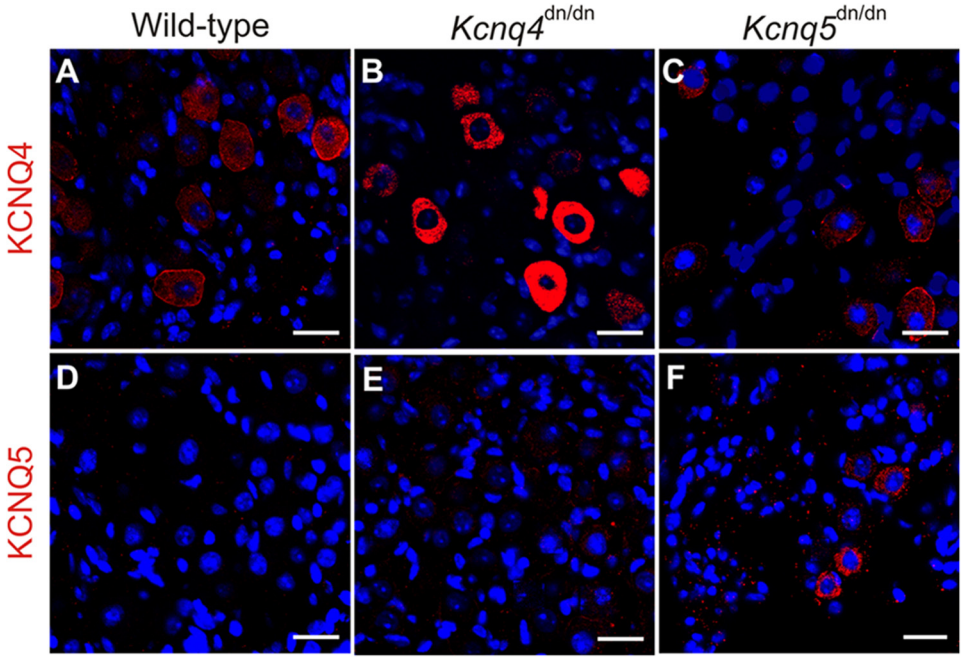

FIGURE 4. **Expression of KCNQ4 and KCNQ5 in vestibular ganglia is increased by trafficking-impaired dominant negative mutations.** Shown is vestibular ganglia staining for KCNQ4 (*A–C*; *red*), or for KCNQ5 (*D–F*; *red*), from wild-type (*A* and *D*), *Kcnq4*$^{dn/dn}$ (*B* and *E*), and *Kcnq5*$^{dn/dn}$ (*C* and *F*). Nuclei were stained with DAPI (*blue*). Note increased cytoplasmic staining for KCNQ4 and KCNQ5 in *Kcnq4*$^{dn/dn}$ and *Kcnq5*$^{dn/dn}$ mice, respectively, without significant effects of the KCNQ4 mutation on KCNQ5 expression and vice versa. *Scale bars*, 20 μm

Similar mutations in KCNQ4 are known to interfere with plasma membrane expression (7, 33, 34). Indeed, neuronal somata in the vestibular ganglion of *Kcnq4*$^{dn/dn}$ mice (5), which express the trafficking-deficient G286S mutant (7), showed intense cytoplasmic KCNQ4 labeling (Fig. 4*B*) compared with WT somata (Fig. 4*A*). KCNQ4 labeling of vestibular end organs disappeared in parallel, as shown for *Kcnq4*$^{dn/dn}$ crista ampullaris in Fig. 5, *A* and *B*. It is instructive to compare these findings with those for the cochlea where KCNQ4 is expressed in outer hair cells (4–6). Unlike vestibular HCs, OHCs displayed detectable levels of the mutant KCNQ4 protein (Fig. 5*D*). Again consistent with impaired trafficking and ER retention, the mutant protein was no longer detected at the basal OHC plasma membrane (Fig. 5*C*), but in a punctate intracellular pattern (Fig. 5*D*).

Our immunohistochemical analysis of mutant mice strongly suggests that KCNQ4 and -5 are expressed in postsynaptic, but not presynaptic membranes of calyx terminals. *In situ* hybridization further strengthened this conclusion. Both *Kcnq4* (Fig. 6, *A* and *B*) and *Kcnq5* (Fig. 6, *C* and *D*) mRNAs were detected in ganglionar cell bodies, but not in vestibular sensory epithelia as would have been expected with an expression in hair cells. Hence, all of our experiments point to a postsynaptic rather than vestibular hair cell expression of KCNQ4 in mice older than 3 weeks.

Consequences of the Loss of KCNQ4 and KCNQ5 for Vestibular Function—*Kcnq4*$^{-/-}$ mice, *Kcnq5*$^{dn/dn}$ mice, and even mice homozygous for both mutations (*Kcnq4*$^{-/-}$/*Kcnq5*$^{dn/dn}$) lacked shaker/waltzer behavior that is indicative of a strong vestibular deficit phenotype as found, *e.g.* in mice lacking the NaK2Cl co-transporter *Nkcc1* (35) or the K^+ β-subunit gene *Kcne1* (36). Both gene products are involved in generating the high endocochlear K^+ concentration that is required for mechanotransduction currents in cochlear and vestibular hair cells.

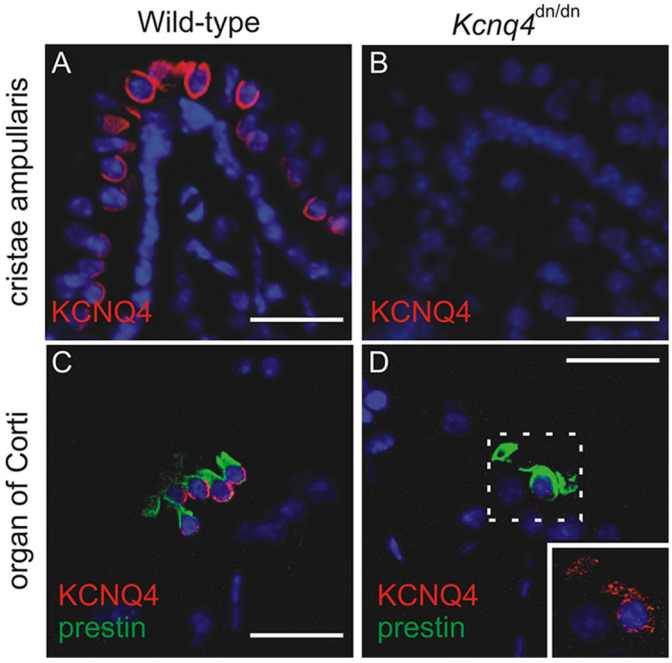

FIGURE 5. **Altered subcellular localization of KCNQ4 in the inner ear of *Kcnq4*$^{dn/dn}$ mice.** *A* and *B*, KCNQ4 (*red*) labeling of the crista ampullaris of wild-type mice (*A*) is abolished in *Kcnq4*$^{dn/dn}$ mice (*B*). *C* and *D*, KCNQ4 (*red*) labeling of the basolateral plasma membrane of prestin-positive (*green*) OHCs of wild-type mice (*C*) is changed to a weak punctate cytoplasmic labeling in *Kcnq4*$^{dn/dn}$ mice (*D*). *Inset*, area enclosed by the *dotted line* is at higher magnification and increased laser intensity. Note the morphological abnormalities of prestin-positive OHCs of *Kcnq4*$^{dn/dn}$ mice due to their incipient degeneration at this age (3 months). Nuclei were labeled with DAPI. *Scale bars*, 20 μm.

To find out whether more subtle vestibular deficits can result from a loss of KCNQ4 and/or KCNQ5 function we measured the VOR in awake, head-restrained *Kcnq4*$^{-/-}$, *Kcnq5*$^{dn/dn}$, and

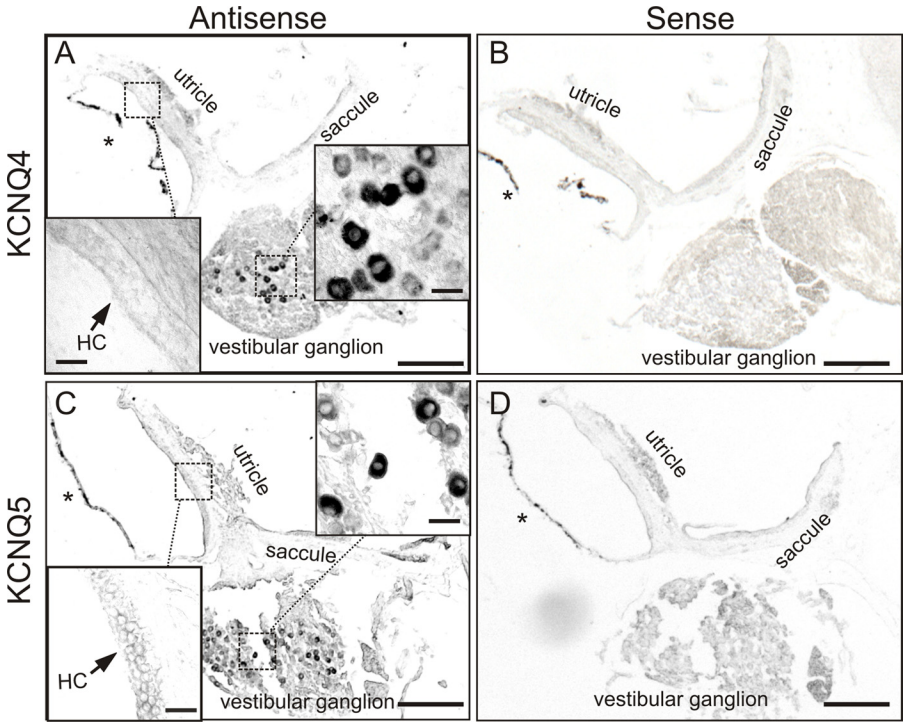

FIGURE 6. **KCNQ4 and KCNQ5 mRNAs are found in adult vestibular ganglia, but not vestibular end organs.** *A* and *C*, *in situ* hybridization of *Kcnq4* (*A*) and *Kcnq5* (*C*) mRNA is shown on vestibular organs of 12–35-week-old mice. *B* and *D*, hybridization with corresponding sense probes provided negative control. *Insets* show higher magnification of the maculae and vestibular ganglion from the areas enclosed by *dotted lines*. *HC* indicates the position of macular hair cells. *Asterisks*, pigmented membranes representing detached epithelial dark cells and which should not be confounded with hybridization signals. *Scale bars*, 200 μm for *main panels*, 20 μm for *insets*.

$Kcnq4^{-/-}/Kcnq5^{dn/dn}$ mice and WT littermates. In this assay, mice are subjected to controlled angular acceleration on a turntable while measuring evoked eye movements with a video camera (Fig. 7, *A* and *B*). These experiments were performed at different rotation frequencies both in the dark and in the light. Stimulus peak velocity was held constant at 25°/s. In the dark, VOR of all four experimental groups (WT, $Kcnq4^{-/-}$, $Kcnq5^{dn/dn}$, and $Kcnq4^{-/-}/Kcnq5^{dn/dn}$) displayed the typical high pass filter behavior, with low gain and a substantial phase lead at low frequencies and high gain and a small phase lag at the high end of the frequency range (Fig. 7, *C* and *D*). Importantly, the VOR gain values of $Kcnq4^{-/-}$ and those of $Kcnq4^{-/-}/Kcnq5^{dn/dn}$ mice were significantly lower compared with those of WT over the entire frequency range (Fig. 7*C*) ($Kcnq4^{-/-}$: $n = 13$, $p < 0.001$; $Kcnq4^{-/-}/Kcnq5^{dn/dn}$: $n = 13$, $p < 0.001$). There was no significant difference in gain values among $Kcnq4^{-/-}$ and $Kcnq4^{-/-}/Kcnq5^{dn/dn}$ mice ($p = 0.531$). The VOR transfer function profile of $Kcnq5^{dn/dn}$ mice showed a moderately increased gain in the stimulus frequency range from 0.5 to 2 Hz, but was only marginally different from WT controls ($p = 0.043$).

In the light, visual feedback elicits an optokinetic reflex that, in addition to the VOR, enhances compensatory eye movement (therefore also referred to as visually enhanced VOR or VVOR). As a consequence, the performance at low frequencies improved to similar levels as observed at high frequencies (Fig. 7, *E* and *F*). The VVOR gain of $Kcnq4^{-/-}$ mice was not significantly different from that in WTs ($p = 0.161$), whereas that of $Kcnq4^{-/-}/Kcnq5^{dn/dn}$ mice was significantly lower than that in WTs ($p = 0.014$). The largest differences in gain and phase of $Kcnq4^{-/-}/Kcnq5^{dn/dn}$ mice were present at the high end of the frequency range, where the contribution of the optokinetic reflex to the total oculomotor performance is the smallest (Fig. 7, *E* and *F*). Rather surprisingly, the $Kcnq5^{dn/dn}$ group showed a higher gain over the entire frequency range (about 0.05 gain increase, $p = 0.003$) compared with WT (Fig. 7*E*).

DISCUSSION

Whereas KCNQ4 K^+ channels are expressed in basal membranes of mouse cochlear OHCs throughout postnatal life (4, 5), in adult vestibular end organs both KCNQ4 and KCNQ5 were only detectable in calyx terminals that innervate type I hair cells. Changed VORs in mice deficient for these channels suggest that these K^+ channels play significant roles in synaptic transmission of vestibular hair cells and/or in the excitability of their afferent neurons. Our findings are relevant for patients with *KCNQ4*-related dominant hearing loss. Some of them present mild vestibular symptoms (13, 37), which, however, cannot be directly compared with the present mouse phenotype because of methodological differences.

For the cochlea, *in situ* hybridization (6), immunohistochemistry (4), and the disappearance of XE991-sensitive K^+ currents in $Kcnq4^{-/-}$ mice (5) provide irrefutable evidence for KCNQ4 being expressed in OHCs. As KCNQ4 was previously immunolocalized to basal poles of cochlear OHCs and type I vestibular HCs, it was assumed that KCNQ4 was expressed in both types of hair cells (4). This notion was strengthened by immunogold electron microscopy (4, 12), which suggested additional postsynaptic expression at calyx terminals. Furthermore, overexpression of a dominant negative KCNQ4 mutant

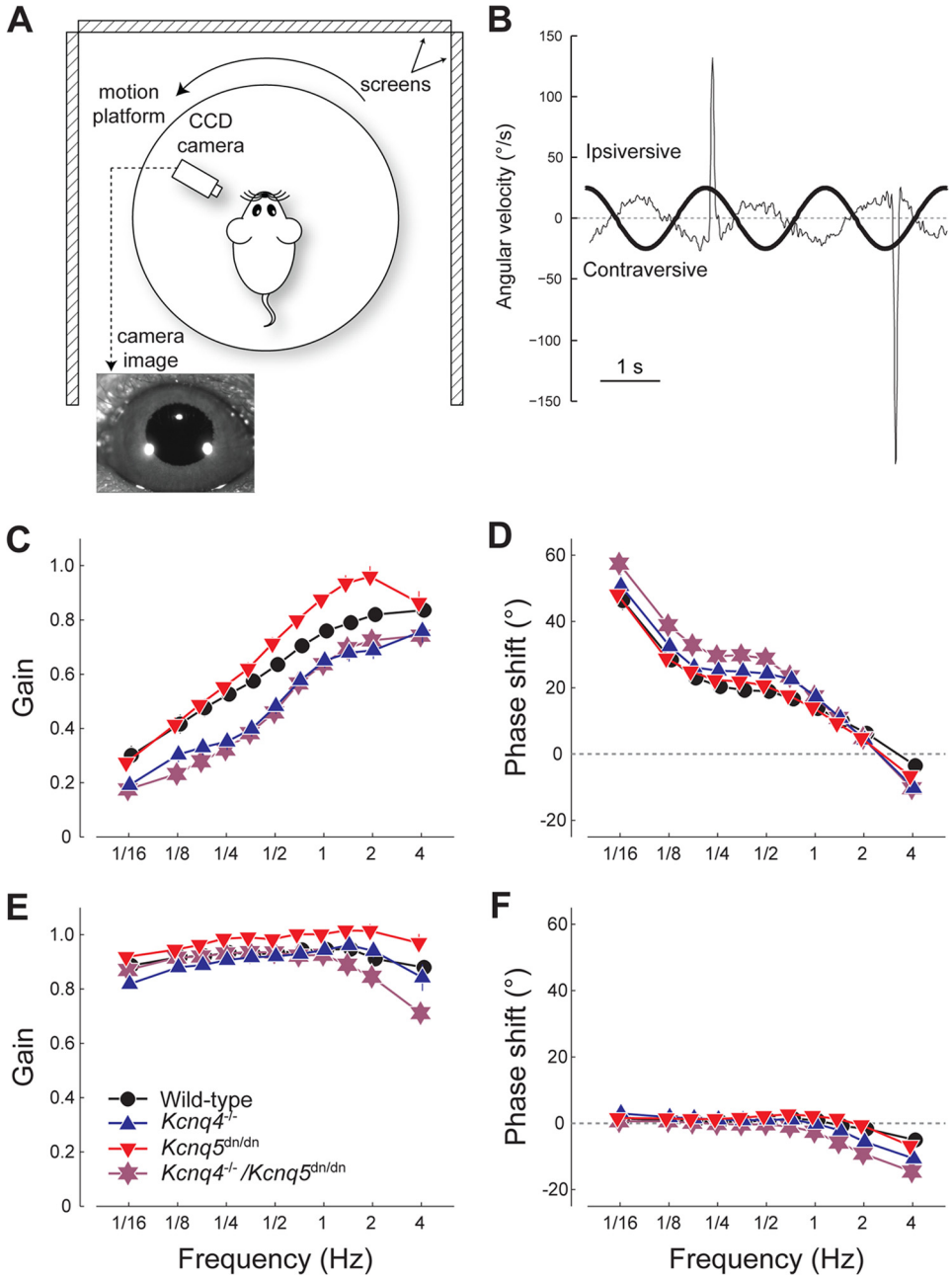

FIGURE 7. **Role of KCNQ4 and KCNQ5 in VORs.** *A*, schematic of experimental setup for VOR measurement (view from above). *B*, example data, showing the VOR eye movement response, including saccades, of a WT mouse (*thin line*) to table movement (*thick line*) at a frequency of 1/2 Hz. *C–F*, transfer function profiles showing gain (*C* and *E*) and phase shift (*D* and *F*) of the VOR performance relative to head velocity for the four experimental groups: WT (*black* ●), *Kcnq4*$^{-/-}$ (*blue* ▲), *Kcnq5*$^{dn/dn}$ (*red* ▼), *Kcnq4*$^{-/-}$/*Kcnq5*$^{dn/dn}$ (*purple star*). *C* and *D*, eye movement performance in the dark (VOR). *E* and *F*, performance of the eye movement response in the light (VOR+OKR). Data represent the mean ± S.E. obtained from $N \geq 13$ animals per group.

suppressed $g_{K,L}$ K^+ currents in type I HCs at P6-P10 (9). This effect likely resulted from a suppression of currents carried by KCNQ4 or other KCNQ subunits with which KCNQ4 can associate.

Later work suggested that KCNQ4 (and possibly KCNQ5) are expressed in type I vestibular HCs only during an early postnatal period (8). Single-cell PCR detected *Kcnq4* and *-5* mRNAs in type I HCs at P1, but their levels declined in parallel to XE991-sensitive HC currents at P14 (8). Membranes of calyx terminals concomitantly started to express XE991-sensitive currents and KCNQ4 protein. The detection by RT-PCR of *Kcnq4* mRNA in P35 maculae (10), however, seems to contradict these findings, but might be caused by small amounts of *Kcnq4* mRNA in dendrites of vestibular neurons.

Our data now show convincingly that in mice older than P28 KCNQ4 and KCNQ5 are expressed in postsynaptic calyx membranes but are not detectable in HCs. Contrasting with the large effects of *Kcnq4* disruption on OHC currents (4), neither loss of *Kcnq4* nor expression of the dominant negative KCNQ5 mutant changed vestibular HC currents of mice older than P28. KCNQ4 and KCNQ5 pore mutant proteins were retained in neuronal somata rather than being trafficked to calyces. *In situ* hybridization performed at that age found mRNAs for both *Kcnq4* and *-5* in vestibular ganglion neurons, but not in vestib-

ular HCs. The apparent discrepancy with earlier work that showed KCNQ4 expression in type I vestibular HCs might be explained by a difference in age and species, with HC expression of KCNQ4 being lost during the 1st week of life in mice, but about 1 week later in rats (1, 8, 38).

Thus the changes of VORs in *Kcnq4*$^{-/-}$ mice are not caused by a direct, cell-intrinsic effect on sensory HCs. VOR measurements depend on cristae ampullares that detect rotational acceleration, whereas our patch clamp analysis was performed in otholithic organs. However, the very similar expression patterns of KCNQ4 and KCNQ5 in both organs strongly suggest similar channel functions in either end organ. In view of the sparse *Kcnq4* expression in brain (4) and its robust postsynaptic expression in calyx synapses, VOR impairment likely originates from altered synaptic transmission and spike initiation in afferent neurons. The presence of a large postsynaptic K^+ conductance that is already active at resting potentials may shunt postsynaptic currents and thereby reduce excitatory postsynaptic potentials (EPSPs). In this scenario, the loss of postsynaptic KCNQ should increase, rather than decrease, the efficiency of synaptic transmission. A decreased electric shunt in the spike initiation zone of afferent neurons will further contribute to a more efficient coupling of HC depolarization to action potential output. Both KCNQ4 and KCNQ5 are partially open at resting voltages and can be further slowly activated by depolarization (5, 6, 14, 15). They may thus contribute to an adaptation of afferent neurons that results in phasic responses (2). Reduced postsynaptic shunting may also decrease the time constant of EPSP decay. The resulting EPSP broadening may affect circuits that compare exactly timed inputs as in the central auditory pathway (39), but is less likely to interfere with the less time-critical signals of vestibular organs.

Synaptic clefts of calyx synapses have extraordinary large areas. Ion concentrations in those clefts must be regulated by transmembrane transport rather than by passive diffusion through the open end of the calyx at the neck of HCs. Both vestibular and cochlear HCs have to cope with apical K^+ influx through mechanosensitive cation channels that occurs at rest and is modulated by mechanical forces. Apical K^+ influx, which depends on the high endolymphatic K^+ concentration, must be balanced by basolateral K^+ efflux. In cochlear OHCs, KCNQ4 provides a major pathway for the basal efflux of K^+ (4–6) which is then removed by the KCC4 K-Cl co-transporter of closely apposed Deiters' cells (40). KCC4 apparently has no role in removing K^+ from the calyx cleft as our unpublished immunohistochemistry did not detect KCC4 in calyx synapses while robustly labeling Deiters' cells. Whereas ion channel(s) mediating K^+ efflux from adult type I vestibular HCs remain to be identified (with a likely contribution of erg channels (8)), we propose that K^+ is removed from the cleft through postsynaptic KCNQ4, KCNQ5, and possibly Kir4.1 K^+ channels, which were also found in type I HC calyces (41). Cellular K^+ uptake through ion channels requires unusual electrochemical K^+ gradients. For example, glial Kir4.1 K^+ channels can take up extracellular K^+ when its concentration rises during neuronal activity (42, 43). Model calculations (44) and experiments (45, 46) suggest a significant activity-dependent rise in the K^+ concentration in clefts of calyx synapses ($[K^+]_{cleft}$). If the postsynaptic membrane is held at sufficiently negative voltages by K^+ channels at the outer calyceal face, postsynaptic K^+ uptake through KCNQ channels appears feasible. Assuming a calyx membrane potential similar to that of cultured vestibular neurons (−70 to −60 mV; (47)) and $[K^+]_i$ = 140 mM, $[K^+]_{cleft}$ would have to rise to >10–15 mM for entering the calyx through K^+ channels. This seems realistic as recent measurements suggested an activity-dependent increase of $[K^+]_{cleft}$ to >50 mM (45).

Hence, loss of KCNQ4 or KCNQ5 may increase $[K^+]_{cleft}$ and thereby depolarize type I hair cells, which may affect their transduction currents (46) or synaptic vesicle exocytosis. However, unlike cochlear OHCs of *Kcnq4*$^{-/-}$ (5) or *Kcc4*$^{-/-}$ (40) mice, vestibular HCs showed no significant degeneration at least up to 10 months of age. Constitutively open K^+ channels in pre- and postsynaptic membranes may also lead to nonquantal neurotransmission between type I hair cells and their cognate afferents (5, 44, 46, 48). Disruption of *Kcnq4* and *Kcnq5* might interfere with this nonconventional type of synaptic communication.

Vestibulo-ocular reflexes were impaired in *Kcnq4*$^{-/-}$ and *Kcnq4*$^{-/-}$/*Kcnq5*$^{dn/dn}$ mice, but not in *Kcnq5*$^{dn/dn}$ mice. The most conspicuous effect was an overall lower VOR gain that was not significantly increased by the additional loss of KCNQ5 function. Interestingly, *Kcnq5*$^{dn/dn}$ mice showed a slight increase in VOR gain in the dark and light. It remains to be shown whether this effect results from the expression of KCNQ5 in the retina (49).

As both KCNQ4 and KCNQ5 channels have roughly similar biophysical properties, the marked difference in their impact on VOR responses in the dark might be caused by differences in global expression levels (that are difficult to determine) or by their differential distribution in vestibular organs. Irregularly firing, phasic afferents innervate type I HCs in the central and striolar regions of cristae and maculae, respectively (27). Exactly these neurons rely predominantly on KCNQ4. By contrast, regularly firing, tonic afferents rather contact peripheral and extrastriolar hair cells (27, 50) which rely more on KCNQ5. Hence, the dependence on KCNQ4 rather than KCNQ5 suggests that vestibular-ocular reflexes depend more on hair cells eliciting phasic rather than tonic responses, which may be related to the fact that these adapting, irregularly firing neurons, together with their upstream hair cells, are more sensitive to mechanical stimulation than the tonic ones.

Acknowledgments—We thank R. Pareja, R. Leben, and P. Seidler for technical assistance.

REFERENCES

1. Rüsch, A., Lysakowski, A., and Eatock, R. A. (1998) Postnatal development of type I and type II hair cells in the mouse utricle: acquisition of voltage-gated conductances and differentiated morphology. *J. Neurosci.* **18,** 7487–7501
2. Jentsch, T. J. (2000) Neuronal KCNQ potassium channels: physiology and role in disease. *Nat. Rev. Neurosci.* **1,** 21–30
3. Soldovieri, M. V., Miceli, F., and Taglialatela, M. (2011) Driving with no brakes: molecular pathophysiology of K_V7 potassium channels. *Physiology* **26,** 365–376
4. Kharkovets, T., Hardelin, J. P., Safieddine, S., Schweizer, M., El-Amraoui, A., Petit, C., and Jentsch, T. J. (2000) KCNQ4, a K^+ channel mutated in a

form of dominant deafness, is expressed in the inner ear and the central auditory pathway. *Proc. Natl. Acad. Sci. U.S.A.* **97,** 4333–4338
5. Kharkovets, T., Dedek, K., Maier, H., Schweizer, M., Khimich, D., Nouvian, R., Vardanyan, V., Leuwer, R., Moser, T., and Jentsch, T. J. (2006) Mice with altered KCNQ4 K^+ channels implicate sensory outer hair cells in human progressive deafness. *EMBO J.* **25,** 642–652
6. Kubisch, C., Schroeder, B. C., Friedrich, T., Lütjohann, B., El-Amraoui, A., Marlin, S., Petit, C., and Jentsch, T. J. (1999) KCNQ4, a novel potassium channel expressed in sensory outer hair cells, is mutated in dominant deafness. *Cell* **96,** 437–446
7. Heidenreich, M., Lechner, S. G., Vardanyan, V., Wetzel, C., Cremers, C. W., De Leenheer, E. M., Aránguez, G., Moreno-Pelayo, M. Á., Jentsch, T. J., and Lewin, G. R. (2012) KCNQ4 K^+ channels tune mechanoreceptors for normal touch sensation in mouse and man. *Nat. Neurosci.* **15,** 138–145
8. Hurley, K. M., Gaboyard, S., Zhong, M., Price, S. D., Wooltorton, J. R., Lysakowski, A., and Eatock, R. A. (2006) M-like K^+ currents in type I hair cells and calyx afferent endings of the developing rat utricle. *J. Neurosci.* **26,** 10253–10269
9. Holt, J. R., Stauffer, E. A., Abraham, D., and Géléoc, G. S. (2007) Dominant-negative inhibition of M-like potassium conductances in hair cells of the mouse inner ear. *J. Neurosci.* **27,** 8940–8951
10. Rocha-Sanchez, S. M., Morris, K. A., Kachar, B., Nichols, D., Fritzsch, B., and Beisel, K. W. (2007) Developmental expression of *Kcnq4* in vestibular neurons and neurosensory epithelia. *Brain Res.* **1139,** 117–125
11. Lysakowski, A., Gaboyard-Niay, S., Calin-Jageman, I., Chatlani, S., Price, S. D., and Eatock, R. A. (2011) Molecular microdomains in a sensory terminal, the vestibular calyx ending. *J. Neurosci.* **31,** 10101–10114
12. Sousa, A. D., Andrade, L. R., Salles, F. T., Pillai, A. M., Buttermore, E. D., Bhat, M. A., and Kachar, B. (2009) The septate junction protein caspr is required for structural support and retention of KCNQ4 at calyceal synapses of vestibular hair cells. *J. Neurosci.* **29,** 3103–3108
13. Marres, H., van Ewijk, M., Huygen, P., Kunst, H., van Camp, G., Coucke, P., Willems, P., and Cremers, C. (1997) Inherited nonsyndromic hearing loss: an audiovestibular study in a large family with autosomal dominant progressive hearing loss related to DFNA2. *Arch. Otolaryngol. Head Neck Surg.* **123,** 573–577
14. Lerche, C., Scherer, C. R., Seebohm, G., Derst, C., Wei, A. D., Busch, A. E., and Steinmeyer, K. (2000) Molecular cloning and functional expression of KCNQ5, a potassium channel subunit that may contribute to neuronal M current diversity. *J. Biol. Chem.* **275,** 22395–22400
15. Schroeder, B. C., Hechenberger, M., Weinreich, F., Kubisch, C., and Jentsch, T. J. (2000) KCNQ5, a novel potassium channel broadly expressed in brain, mediates M-type currents. *J. Biol. Chem.* **275,** 24089–24095
16. Tzingounis, A. V., Heidenreich, M., Kharkovets, T., Spitzmaul, G., Jensen, H. S., Nicoll, R. A., and Jentsch, T. J. (2010) The KCNQ5 potassium channel mediates a component of the afterhyperpolarization current in mouse hippocampus. *Proc. Natl. Acad. Sci. U.S.A.* **107,** 10232–10237
17. Lysakowski, A., Alonto, A., and Jacobson, L. (1999) Peripherin immunoreactivity labels small diameter vestibular "bouton" afferents in rodents. *Hear. Res.* **133,** 149–154
18. Rickheit, G., Maier, H., Strenzke, N., Andreescu, C. E., De Zeeuw, C. I., Muenscher, A., Zdebik, A. A., and Jentsch, T. J. (2008) Endocochlear potential depends on Cl^- channels: mechanism underlying deafness in Bartter syndrome IV. *EMBO J.* **27,** 2907–2917
19. Braissant, O., and Wahli, W. (1998) Differential expression of peroxisome proliferator-activated receptor-α, -β, and -γ during rat embryonic development. *Endocrinology* **139,** 2748–2754
20. Gaboyard, S., Chabbert, C., Travo, C., Bancel, F., Lehouelleur, J., Yamauchi, D., Marcus, D. C., and Sans, A. (2005) Three-dimensional culture of newborn rat utricle using an extracellular matrix promotes formation of a cyst. *Neuroscience* **133,** 253–265
21. Wulff, P., Schonewille, M., Renzi, M., Viltono, L., Sassoè-Pognetto, M., Badura, A., Gao, Z., Hoebeek, F. E., van Dorp, S., Wisden, W., Farrant, M., and De Zeeuw, C. I. (2009) Synaptic inhibition of Purkinje cells mediates consolidation of vestibulo-cerebellar motor learning. *Nat. Neurosci.* **12,** 1042–1049
22. Stahl, J. S., van Alphen, A. M., and De Zeeuw, C. I. (2000) A comparison of video and magnetic search coil recordings of mouse eye movements. *J. Neurosci. Methods* **99,** 101–110
23. Stahl, J. S. (2002) Calcium channelopathy mutants and their role in ocular motor research. *Ann. N.Y. Acad. Sci.* **956,** 64–74
24. Bal, M., Zhang, J., Zaika, O., Hernandez, C. C., and Shapiro, M. S. (2008) Homomeric and heteromeric assembly of KCNQ (K_v7) K^+ channels assayed by total internal reflection fluorescence/fluorescence resonance energy transfer and patch clamp analysis. *J. Biol. Chem.* **283,** 30668–30676
25. Schroeder, B. C., Kubisch, C., Stein, V., and Jentsch, T. J. (1998) Moderate loss of function of cyclic AMP-modulated KCNQ2/KCNQ3 K^+ channels causes epilepsy. *Nature* **396,** 687–690
26. Wang, H. S., Pan, Z., Shi, W., Brown, B. S., Wymore, R. S., Cohen, I. S., Dixon, J. E., and McKinnon, D. (1998) KCNQ2 and KCNQ3 potassium channel subunits: molecular correlates of the M channel. *Science* **282,** 1890–1893
27. Goldberg, J. M., Lysakowski, A., and Fernández, C. (1992) Structure and function of vestibular nerve fibers in the chinchilla and squirrel monkey. *Ann. N.Y. Acad. Sci.* **656,** 92–107
28. Rennie, K. J., Weng, T., and Correia, M. J. (2001) Effects of KCNQ channel blockers on K^+ currents in vestibular hair cells. *Am. J. Physiol. Cell Physiol.* **280,** C473–480
29. Correia, M. J., and Lang, D. G. (1990) An electrophysiological comparison of solitary type I and type II vestibular hair cells. *Neurosci. Lett.* **116,** 106–111
30. Rüsch, A., and Eatock, R. A. (1996) A delayed rectifier conductance in type I hair cells of the mouse utricle. *J. Neurophysiol.* **76,** 995–1004
31. Chen, J. W., and Eatock, R. A. (2000) Major potassium conductance in type I hair cells from rat semicircular canals: characterization and modulation by nitric oxide. *J. Neurophysiol.* **84,** 139–151
32. Søgaard, R., Ljungstrøm, T., Pedersen, K. A., Olesen, S. P., and Jensen, B. S. (2001) KCNQ4 channels expressed in mammalian cells: functional characteristics and pharmacology. *Am. J. Physiol. Cell Physiol.* **280,** C859–866
33. Mencía, A., González-Nieto, D., Modamio-Høybjør, S., Etxeberría, A., Aránguez, G., Salvador, N., Del Castillo, I., Villarroel, A., Moreno, F., Barrio, L., and Moreno-Pelayo, M. A. (2008) A novel KCNQ4 pore-region mutation (p.G296S) causes deafness by impairing cell-surface channel expression. *Hum. Genet.* **123,** 41–53
34. Kim, H. J., Lv, P., Sihn, C. R., and Yamoah, E. N. (2011) Cellular and molecular mechanisms of autosomal dominant form of progressive hearing loss, DFNA2. *J. Biol. Chem.* **286,** 1517–1527
35. Delpire, E., Lu, J., England, R., Dull, C., and Thorne, T. (1999) Deafness and imbalance associated with inactivation of the secretory Na-K-2Cl co-transporter. *Nat. Genet.* **22,** 192–195
36. Vetter, D. E., Mann, J. R., Wangemann, P., Liu, J., McLaughlin, K. J., Lesage, F., Marcus, D. C., Lazdunski, M., Heinemann, S. F., and Barhanin, J. (1996) Inner ear defects induced by null mutation of the *isk* gene. *Neuron* **17,** 1251–1264
37. De Leenheer, E. M., Huygen, P. L., Coucke, P. J., Admiraal, R. J., van Camp, G., and Cremers, C. W. (2002) Longitudinal and cross-sectional phenotype analysis in a new, large Dutch DFNA2/KCNQ4 family. *Ann. Otol. Rhinol. Laryngol.* **111,** 267–274
38. Géléoc, G. S., Risner, J. R., and Holt, J. R. (2004) Developmental acquisition of voltage-dependent conductances and sensory signaling in hair cells of the embryonic mouse inner ear. *J. Neurosci.* **24,** 11148–11159
39. Trussell, L. O. (1999) Synaptic mechanisms for coding timing in auditory neurons. *Annu. Rev. Physiol.* **61,** 477–496
40. Boettger, T., Hübner, C. A., Maier, H., Rust, M. B., Beck, F. X., and Jentsch, T. J. (2002) Deafness and renal tubular acidosis in mice lacking the K-Cl co-transporter *Kcc4*. *Nature* **416,** 874–878
41. Udagawa, T., Tatsumi, N., Tachibana, T., Negishi, Y., Saijo, H., Kobayashi, T., Yaguchi, Y., Kojima, H., Moriyama, H., and Okabe, M. (2012) Inwardly rectifying potassium channel Kir4.1 is localized at the calyx endings of vestibular afferents. *Neuroscience* **215,** 209–216
42. Neusch, C., Papadopoulos, N., Müller, M., Maletzki, I., Winter, S. M., Hirrlinger, J., Handschuh, M., Bähr, M., Richter, D. W., Kirchhoff, F., and Hülsmann, S. (2006) Lack of the Kir4.1 channel subunit abolishes K^+ buffering properties of astrocytes in the ventral respiratory group: impact on extracellular K^+ regulation. *J. Neurophysiol.* **95,** 1843–1852

43. Bay, V., and Butt, A. M. (2012) Relationship between glial potassium regulation and axon excitability: a role for glial Kir4.1 channels. *Glia* **60,** 651–660
44. Goldberg, J. M. (1996) Theoretical analysis of intercellular communication between the vestibular type I hair cell and its calyx ending. *J. Neurophysiol.* **76,** 1942–1957
45. Lim, R., Kindig, A. E., Donne, S. W., Callister, R. J., and Brichta, A. M. (2011) Potassium accumulation between type I hair cells and calyx terminals in mouse crista. *Exp. Brain Res.* **210,** 607–621
46. Contini, D., Zampini, V., Tavazzani, E., Magistretti, J., Russo, G., Prigioni, I., and Masetto, S. (2012) Intercellular K^+ accumulation depolarizes type I vestibular hair cells and their associated afferent nerve calyx. *Neuroscience* **227,** 232–246
47. Kalluri, R., Xue, J., and Eatock, R. A. (2010) Ion channels set spike timing regularity of mammalian vestibular afferent neurons. *J. Neurophysiol.* **104,** 2034–2051
48. Goldberg, J. M. (1996) Transmission between the type I hair cell and its calyx ending. *Ann. N.Y. Acad. Sci.* **781,** 474–488
49. Zhang, X., Yang, D., and Hughes, B. A. (2011) KCNQ5/K_v7.5 potassium channel expression and subcellular localization in primate retinal pigment epithelium and neural retina. *Am. J. Physiol. Cell Physiol.* **301,** C1017–1026
50. Eatock, R. A., Xue, J., and Kalluri, R. (2008) Ion channels in mammalian vestibular afferents may set regularity of firing. *J. Exp. Biol.* **211,** 1764–1774

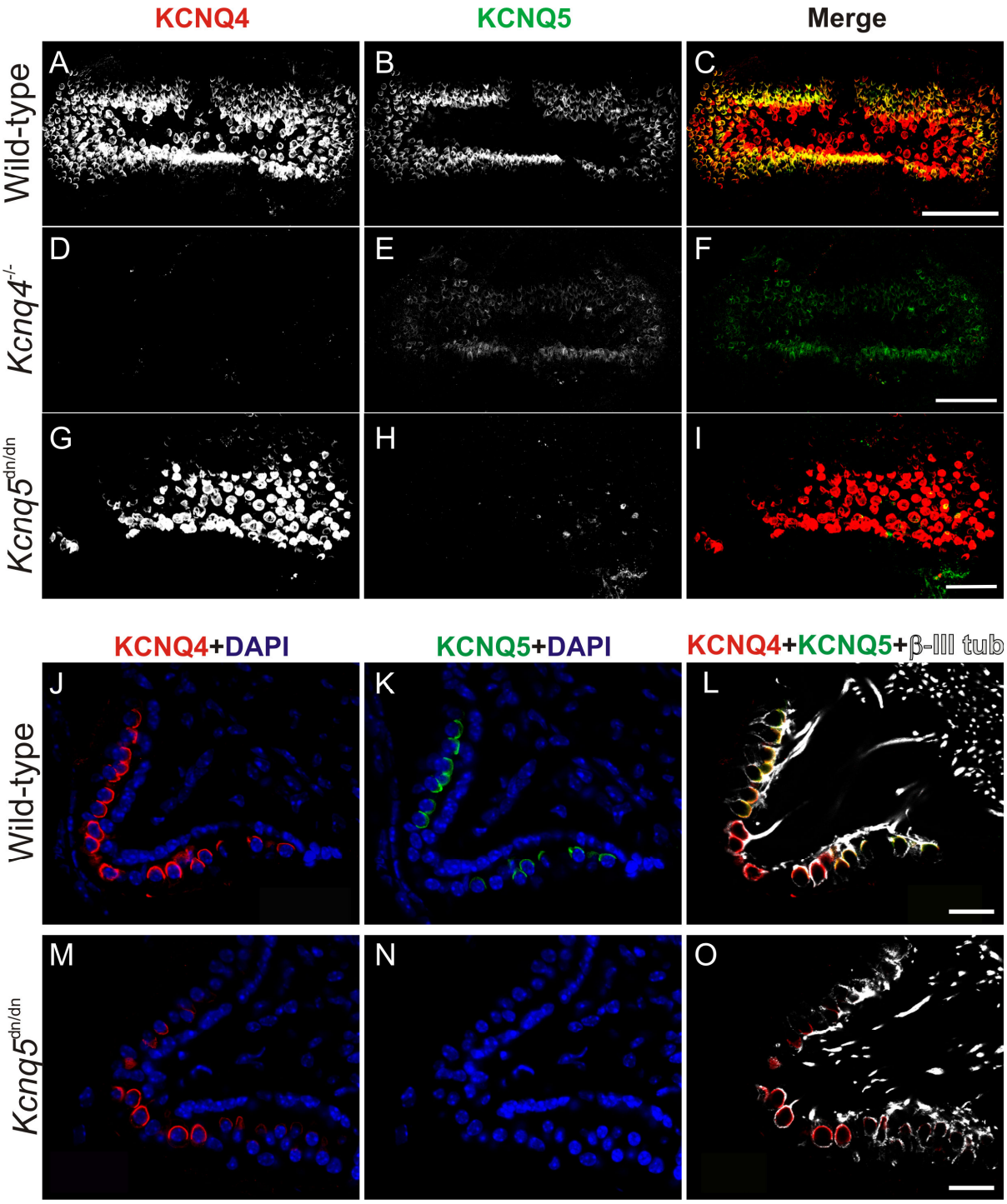

Supplementary Figure S1. KCNQ4 and KCNQ5 in mouse cristae ampullaris. A-I, whole-mount preparations of cristae ampullares from WT (A-C), *Kcnq4*$^{-/-}$ (D-F) and *Kcnq5*$^{dn/dn}$ (G-I) mice stained with antibodies against KCNQ4 (left panel) and KCNQ5 (middle panel). Merged pictures are shown in the right panel C,F,I (KCNQ4, red; KCNQ5, green). Scale bars, 100 µm for A-F and 40 µm for G-I. Several confocal layers were superimposed to obtain images of the whole organs. J-O, slice preparation of cristae ampullares from WT (J-L) and *Kcnq5*$^{dn/dn}$ (M-O) mice. 8 µm sections were stained with antibodies against KCNQ4 (red), KCNQ5 (green) and β-III tubulin (grey). Note more restricted KCNQ4 expression pattern in *Kcnq5*$^{dn/dn}$ cristae. Nuclei were stained with DAPI (blue). Scale bars for J-O 20 µm.

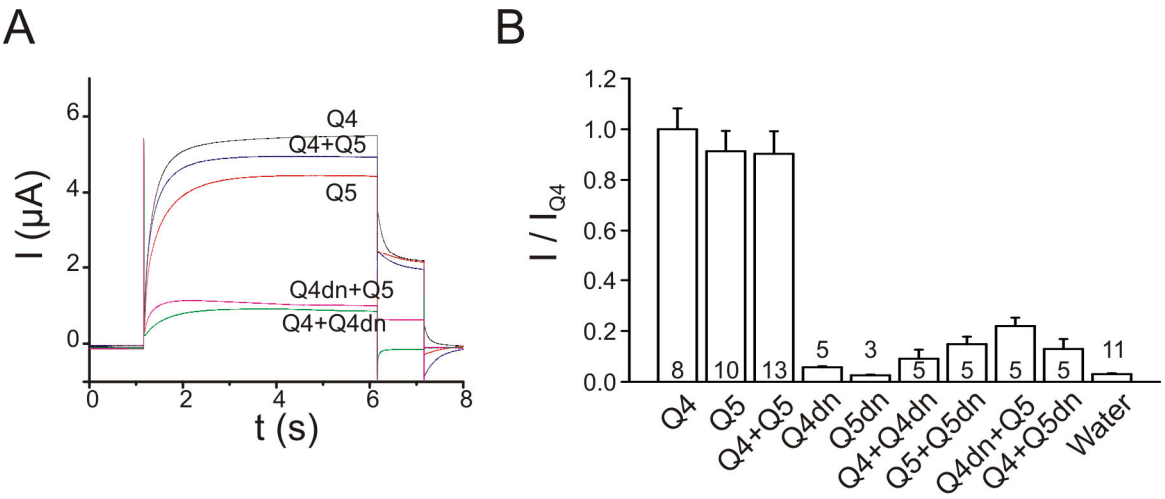

Supplementary Figure S2. KCNQ4 and KCNQ5 form heteromers *in vitro*. A. Typical currents of *Xenopus* oocytes previously injected with RNA encoding KCNQ4 (Q4), KCNQ5 (Q5), KCNQ4(G285S) (Q4dn) and KCNQ5(G278S) (Q5dn). The total amount of injected cRNA was 20 ng. Mixtures were injected at 1:1 ratios. Oocytes were clamped to -80 mV and then depolarized to +20 mV for 5 seconds, followed by a 1-sec step to -20 mV and a return to -80 mV. B. Averaged currents (at the end of the +20 mV voltage step) of experiments like in (A), but including also expression of the dominant negative KCNQ5(G278S) mutant. Note that dominant negative mutants not only suppressed currents from the same subunit, but also from the other one, demonstrating formation of KCNQ4-KCNQ5 heteromers. 1:1 KCNQ4/KCNQ5 co-injection did not increase current amplitudes. Currents from two batches of oocytes were normalized to the respective mean KCNQ4 current and averaged. Error bars, SEM. Numbers in or above columns indicate the number of measured oocytes.

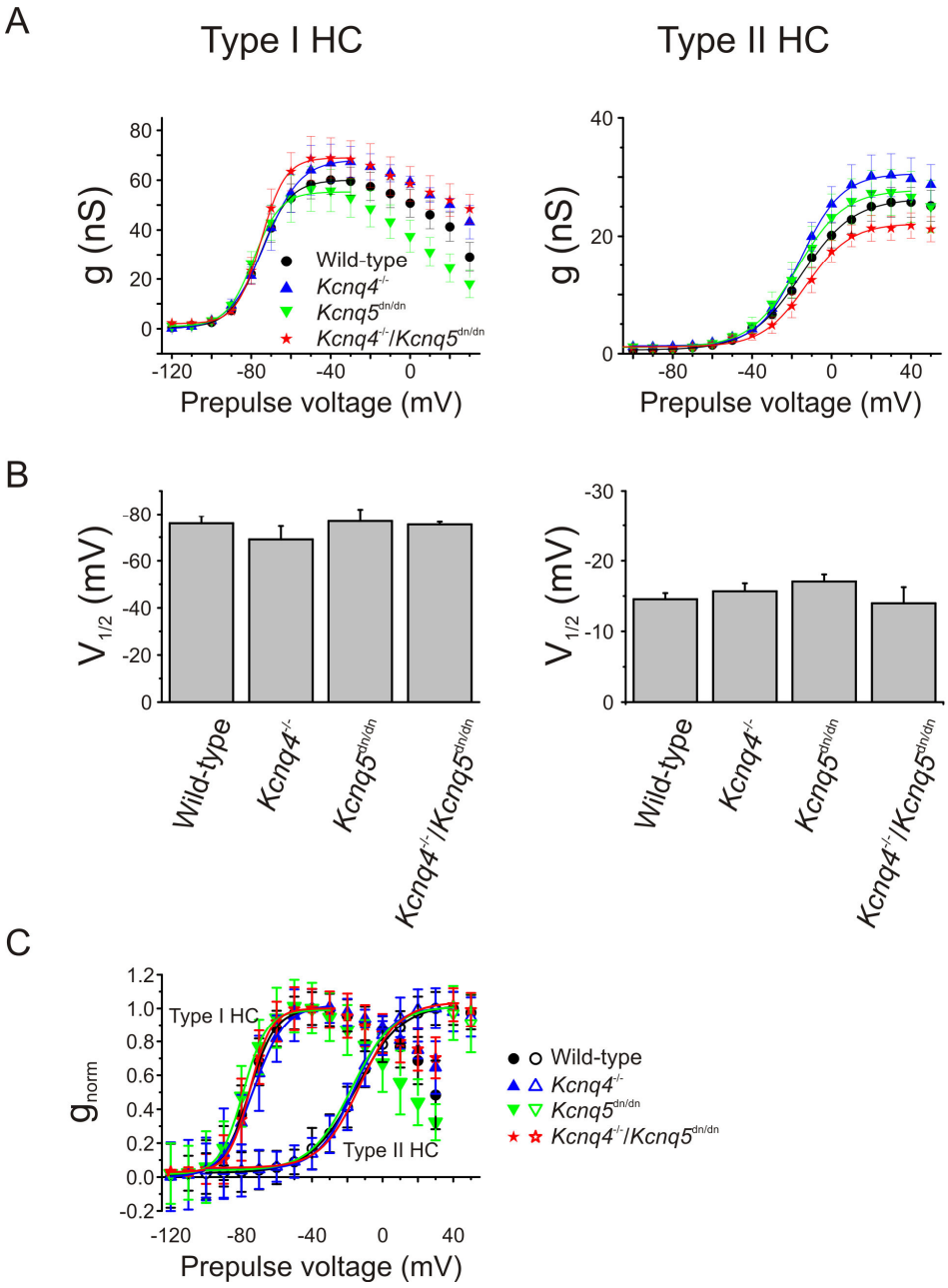

Supplementary Figure S3. Activation curves obtained from tail currents from type I and type II HCs of WT and the 3 mouse models. **A.** Activation curves for type I (left) and type II (right) HCs for WT (black circles) and *Kcnq4*$^{-/-}$ (Upper blue triangle), *Kcnq5*$^{dn/dn}$ (lower green triangle) and *Kcnq4*$^{-/-}$/*Kcnq5*$^{dn/dn}$ (red star) mice. The tail currents at the step to -30 mV was calculated and converted to conductance (g) by dividing the driving force (55 mV and 43 mV for type I and type II HCs, respectively) and then plotted versus the previous step potentials. Data were fit with the Boltzmann equation. Bars indicate SEM. **B**. Half-maximal voltage of activation ($V_{1/2}$) obtained from Boltzman fits for WT, *Kcnq4*$^{-/-}$, *Kcnq5*$^{dn/dn}$ and *Kcnq4*$^{-/-}$/*Kcnq5*$^{dn/dn}$ mice for type I (left) and type II (right) HCs. Fits were done individually for each experiment and then averaged. Differences in $V_{1/2}$ were statistically not significant with respect to WT. **C.** Normalized conductance (g_{norm}) for the curves plotted in A for type I (closed symbols) and type II (open symbols) HCs.